

A Soft-input Soft-output Polar Decoding Algorithm for Turbo-detection in MIMO-Aided 5G New Radio

Zeynep B. Kaykac Egilmez, Luping Xiang, Robert G. Maunder, *Senior Member, IEEE*, and Lajos Hanzo, *Fellow, IEEE*

Abstract—Soft-Input Soft-Output (SISO) polar decoding algorithms, such as Belief Propagation (BP) and Soft Cancellation (SCAN) polar decoding, offer iteration capability for facilitating turbo-style detection. However, at lower Signal-to-Noise Ratios (SNRs), the performance of the BP and SCAN decoders is about 1.5 dB and 0.5 dB worse than that of the state-of-the-art hard-decision Successive Cancellation List (SCL) decoding algorithm, respectively, despite iteratively exchanging information with a Multiple Input Multiple Output (MIMO) detector. Motivated by this gap, we conceive a novel G-SCAN polar decoder, which generates both soft-decision and hard-decision outputs. This is achieved by intrinsically amalgamating a list decoder with a novel SISO decoder. These soft-decision outputs may be used for turbo-detection, but they also support the hard-decision outputs of the SCL algorithm for achieving superior block error rate (BLER) performance. As a result of these benefits, the proposed G-SCAN algorithm using a list size of $L = 2$ offers around 1dB BLER gain compared to the conventional hard-decision SCL decoder relying on $L = 32$. Furthermore, we have carried out its Extrinsic Information Transfer (EXIT) chart analysis, and characterized the performance vs. the complexity of the proposed G-SCAN algorithm, and compared it to various soft- and hard-decision output benchmarks for a wide variety of different rate-matching modes and block lengths. Furthermore, in order to reduce the complexity of the proposed algorithm, a novel Cyclic Redundancy Check (CRC)-aided G-SCAN algorithm is also proposed, which facilitates early termination and improves the BLER performance.

Index Terms—Successive Cancellation List (SCL) decoding, Soft Cancellation (SCAN) decoding, turbo-detection, iterative polar decoding, soft-in soft-out, 5G, NR, MIMO-detection.

I. INTRODUCTION

The 3rd Generation Partnership Project's (3GPP) Long Term Evolution (LTE) [1] standard adopted turbo codes for channel coding in data channels, and Tail-Biting Convolutional Codes (TBCC) for the control channels. Furthermore, 4th Generation (4G) LTE combined these channel codes with Multiple Input Multiple Output (MIMO) and Orthogonal Frequency Division Multiplexing (OFDM) techniques attaining MIMO gains in practical channels. Additionally, state-of-the-art advanced receiver schemes were combined with Soft-Input Soft-Output (SISO) versions of turbo decoding and MIMO detection in order to realise iterative turbo-detection [2]–[5]. More explicitly,

The authors are with the School of Electronics and Computer Science, University of Southampton, Southampton SO17 1BJ, U.K. (e-mail: {zbk1y15, lx1g15, rm, lh}@ecs.soton.ac.uk).

L. Hanzo would like to acknowledge the financial support of the Engineering and Physical Sciences Research Council projects EP/P034284/1 and EP/P003990/1 (COALESCE) as well as of the European Research Council's Advanced Fellow Grant QuantCom (Grant No. 789028)

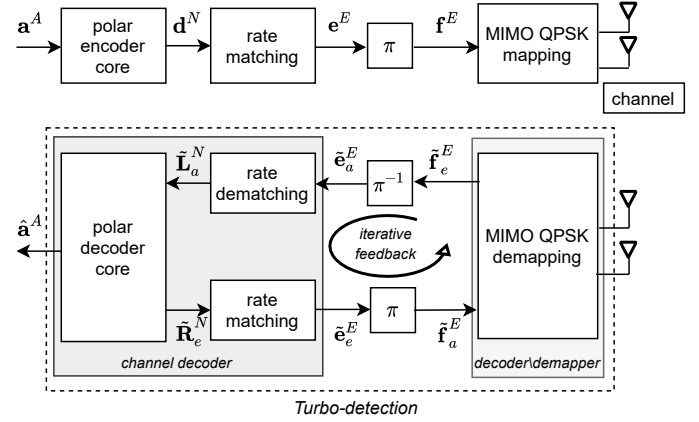


Fig. 1. Illustration of the turbo-detection principle wherein a SISO channel decoder and a SISO MIMO detector iteratively exchange extrinsic information.

during the turbo-detection, the soft values pertaining to the encoded transmitted bits may then be expressed in log-likelihood ratios (LLRs), which may be iteratively exchanged between the SISO turbo decoder [2], [3] and MIMO detector [5]–[7]. In successive iterations, the turbo decoder and MIMO detector alternately generate new sequences of extrinsic LLRs which are iteratively exchanged [2], as shown in Figure 1. In successive iterations, the soft-decision estimates of transmitted bits become more accurate as more soft-information is exchanged [6]. It has been shown that this turbo-detection approach [4] offers significant performance gains in 4G LTE, when iterating between the SISO turbo decoder [3] and a 4x4 MIMO detector, providing 4 to 5 dB gain over conventional non-iterative Minimum Mean Square Error (MMSE) detection, and 2 to 3 dB gain over Successive Interference Cancellation (SIC) in the case of high order modulation schemes [6].

More recently, the 5th Generation (5G) 3GPP New Radio (NR) standard [16] has adopted Low-Density Parity-Check (LDPC) codes for data channels and polar codes for control channels, which offer significant coding gains compared to the codes used in 4G LTE [17]. In terms of the turbo-detection approach, a similar opportunity to that of 4G LTE is offered for LDPC in 5G NR, and these techniques have been extensively explored in [18]–[20], because LDPC decoders naturally provide a soft-in soft-out capability, which is conducive to turbo-MIMO detection. In the case of the control channels, turbo-detection may be potentially executed using SISO polar decoders, such as Belief Propagation (BP) [8],

TABLE I
A TABLE OF ABBREVIATIONS AND NOTATIONS.

Acronyms		Acronyms		Notations	
BP	Belief Propagation	MMSE	Minimum Mean Square Error	A	Number of bits in an information block
BLER	Block Error Ratio	NR	New Radio	I_{max_o}	Maximum number of outer iterations performed for turbo-detection
CA-polar	CRC-Aided polar code	OFDM	Orthogonal Frequency Division Multiplexing	I_{max_i}	Maximum number of inner iterations performed by decoder
CRC	Cyclic Redundancy Check	QPSK	Quadrature Phase Shift Keying	P	Number of CRC bits appended to an information block
EXIT	Extrinsic Information Transfer	TBCC	Tail-Biting Convolutional Codes	L	SCL decoder list size
FAR	False Alarm Rate	SC	Successive Cancellation	E	Number of bits in an encoded block segment
LDPC	Low Density Parity Check	SCL	Successive Cancellation List	N	Number of bits encoded by a polar encoder core (must be a power of 2)
LLR	Logarithmic Likelihood Ratio	SISO	Soft-Input Soft-Output	$\tilde{\mathbf{X}}_a^N$ or $\tilde{\mathbf{X}}_a^E$	N or E number of <i>a-priori</i> LLRs
LTE	Long Term Evolution	SIC	Successive Interference Cancellation	$\tilde{\mathbf{X}}_e^N$ or $\tilde{\mathbf{X}}_e^E$	N or E number of extrinsic LLRs
MIMO	Multiple Input Multiple Output	SNR	Signal-to-Noise Ratio	\mathbf{x}^N or \mathbf{x}^E	N or E number of bits
ML	Maximum Likelihood	3GPP	Third Generation Partnership Project	$\hat{\mathbf{x}}^A$	A number of decoded bits

TABLE II
CONTRASTING OUR CONTRIBUTION TO THE STATE-OF-THE-ART POLAR DECODERS, AS WELL AS WITH EXISTING SURVEYS.

Contributions	This work	BP [8]	SCAN [9]	SCL [10]	SC [11]	CA-SCL [12]	BPL [13]	CA-BPL [14]	Soft-SCL [15]
Soft information outputs	✓	✓	✓				✓	✓	✓
Hard information outputs	✓			✓	✓	✓			✓
Turbo-detection application	✓								✓
5G NR polar code application	✓						✓	✓	✓
Rate matching analysis	✓								✓
Analytically driven algorithm	✓	✓	✓	✓	✓	✓	✓	✓	
Offers an CRC-aided algorithm	✓					✓		✓	✓
EXIT chart analysis	✓								

[21] and Soft Cancellation (SCAN) [9] algorithms. However, these SISO algorithms are unable to achieve the same Block Error Rate (BLER) performance as the hard-decision output Successive Cancellation List (SCL) decoder [10], even when they iteratively exchange soft-information with a MIMO detector, especially at low Signal-to-Noise Ratios (SNRs). The combination of a list size $L = 32$ SCL polar decoder with non-iterative MIMO detection offers 0.5 dB gain over SCAN decoding iterated with MIMO detection, as well as around 1.5 dB gain over min-sum BP decoding iterated with MIMO detection, at low SNRs. However, despite offering the best performance, this SCL decoding scheme can only benefit from one-shot MIMO detection, since it does not have a soft output capability, which is required for attaining iterative gains in turbo-detection. Hence, an opportunity is presented to further improve the SCL decoder by providing it with a soft-decision output capability, which will then result in further iterative MIMO detection gains.

Motivated by this, we propose a beneficial scheme that exploits this opportunity and offers the best of both worlds, where our polar decoding algorithm generates soft outputs for attaining iterative turbo-detection gains, as well as hard outputs for improving the SCL BLER performance. We refer to our proposed soft-in soft-out list decoding algorithm as the G-SCAN and we demonstrate that it has superior performance to conventional turbo-detected BP and SCAN polar decoders, as well as to conventional (i.e. non-turbo) detected state-of-the-art hard-decision SCL polar decoders. For example, the proposed G-SCAN algorithm having a list size of $L = 2$ and iteratively exchanging its information with a 2x2 Quadrature Phase Shift Keying (QPSK) MIMO detector offers about 1 dB gain over the conventional $L = 32$ SCL decoder, when communicating over an uncorrelated narrowband Rayleigh fading channel. Furthermore, in order to reduce the complexity of the proposed G-SCAN algorithm, we propose a novel Cyclic Redundancy Check (CRC)-aided G-SCAN polar decoder algorithm. Here,

the CRC is exploited for early termination of the iterations, and also for CRC-aided list decoding, which improves the BLER performance.

We boldly and explicitly contrast our contributions to the state-of-the-art polar decoders, as well as to the recently introduced list decoding based SISO polar decoders in Table I. More specifically, the novel contributions of this paper may be summarised as follows:

- Firstly, our proposed algorithm offers better error correction performance than the schemes of [8] to [14], and the same BLER performance as [15].
- Furthermore, while [15] proposed a soft-decision list decoder using a BP scheme, in contrast to the scheme we proposed here, it adopted a heuristic approach which is not supported by an analytic motivation. Hence, our scheme improves the robustness in diverse use cases.
- Furthermore, it is a requirement of the 5G NR polar codes to support diverse information block lengths and codeword lengths [22]. This inspired us to investigate different rate matching modes such as repetition, shortening and puncturing for our turbo-detection approach. We will show that the proposed G-SCAN algorithms offer superior performance in each rate matching mode over the iterative soft-decision output benchmarks, as well as over the conventional hard-decision output benchmarks.
- Finally, the Extrinsic Information Transfer (EXIT) chart analysis of turbo-detected 5G NR polar codes is provided for the first time by considering all supported rate matching modes of a 2x2 MIMO scheme.
- Additionally, the detailed contribution of these recently introduced polar decoders and their error correction performance is compared in Table III at a glance.

The rest of the paper is organized as follows. Section II introduces details of the proposed G-SCAN polar decoder algorithm, as well as of the proposed CA-G-SCAN polar decoder algorithm. Sections III details the schedule of turbo-detected MIMO system model. Then, Sections IV, V and VI introduce our simulation results and analysis by considering different rate matching modes and code block lengths. Explicitly, the EXIT chart analysis, complexity analysis and performance analysis of the proposed G-SCAN decoder, and a wide variety of soft- and hard-decision output benchmarks have been provided, respectively. Finally, Section VII offers our conclusions.

II. PROPOSED POLAR DECODER SCHEME

This section describes the proposed G-SCAN algorithm. More specifically, Section II-A details its decoding schedule and the equations used by the G-SCAN algorithm, while considering the similarities and differences with respect to other common polar decoding algorithms, such as SC [11], SCL [10], and SCAN [9] decoders. Following this, Section II-B introduces a CA-G-SCAN algorithm, in order to reduce the complexity of the proposed algorithm.

A. Proposed G-SCAN Polar Decoder Algorithm

As mentioned in Section I, the proposed G-SCAN algorithm can be used as SISO channel decoder to iterate with a SISO

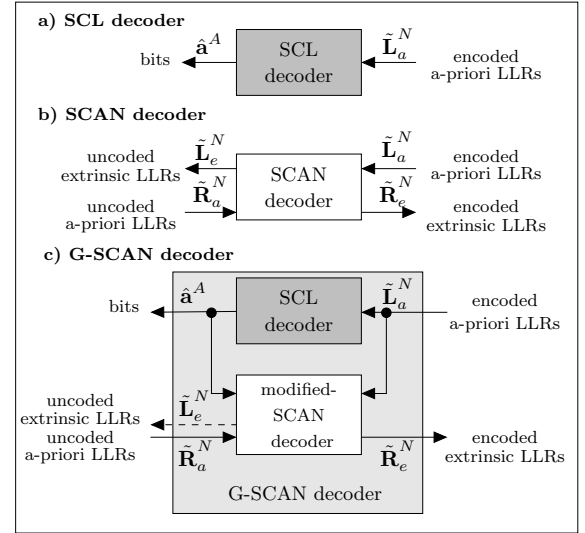


Fig. 2. Block diagram of the proposed G-SCAN decoder, in comparison to that of the SCL and the SCAN decoders.

detector, such as the QPSK MIMO detector. During the initial iterations, the proposed G-SCAN decoder is employed to convert a block comprising N encoded *a-priori* LLRs $\tilde{\mathbf{L}}_a^N$ into a block comprising N encoded extrinsic LLRs $\tilde{\mathbf{R}}_e^N$ which will be iteratively exchanged with the SISO detector. Here, N represents the encoded block length, which must be a power of 2. Then, in the final iteration, the proposed G-SCAN decoder is employed a conventional SCL decoder [10] to convert the block of N encoded *a-priori* LLRs $\tilde{\mathbf{L}}_a^N$ into a block of A decoded bits $\hat{\mathbf{a}}^A$, where the A represents the number of decoded information bits.

To elaborate on the initial iterations, the proposed G-SCAN polar decoder combines two main steps, as shown in Figure 2. In the first step, the decoder takes a block of encoded *a-priori* LLRs $\tilde{\mathbf{L}}_a^N$ as its input and applies the SCL algorithm as usual [10], which selects the best block of decoded bits $\hat{\mathbf{a}}^A$ among a list of L candidates. In the second step, this block comprising A decision bits is interleaved with $(N - A)$ frozen bits, which are inserted into a modified-SCAN decoder together with the same block of N encoded *a-priori* LLRs $\tilde{\mathbf{L}}_a^N$, that was provided to the SCL decoder as its input, for generating a block of encoded extrinsic LLRs $\tilde{\mathbf{R}}_e^N$. Optionally, the proposed G-SCAN decoder may also provide a block of uncoded extrinsic LLRs $\tilde{\mathbf{L}}_e^N$, which represent soft-decision outputs of the modified-SCAN decoder. Before deciding to use the decoding candidate having the best path metric produced by the SCL decoder as the basis of the modified-SCAN algorithm, we considered a variety of different alternatives for how we can leverage the hard-decision output of the SCL decoder. For example, we considered adopting only a subset of N bit decisions, where all of the L decoding candidates agree on the value of that particular bit. However, we have found that this gives inferior performance to that of the proposed scheme, which ultimately dictated our choice.

More specifically, the two components of the proposed G-

SCAN decoder, namely the SCL decoder and the modified-SCAN decoder beneficially complement each other. Explicitly, the SCL decoder can only provide hard-decision outputs, but offers superior error correction capability. By contrast, the SCAN decoder generates a soft-decision output, but has a lower error correction capability than the SCL decoder. However, the modified-SCAN decoder can process the SCL decoder's output, which allows them to work together to deliver the best of both worlds, as mentioned in Section I.

Similar to other polar decoders [23], the proposed G-SCAN polar decoder core can be operated on the basis of the same factor graph that is used in the polar encoder core, which is exemplified in Figure 3a for the case of $N = 8$. In general, a factor graph comprises $\frac{Nn}{2}$ unit factor graphs and Nn nodes where $N = 2^n$, with each unit factor graph being connected to four nodes. Here, n represents the number of the layers in the factor graph, where each layer comprises $N/2$ partial sum (XOR) gates, as illustrated in Figure 3a. The operation of the SCL decoder component of the G-SCAN on the basis of the polar code factor graph is well understood and detailed in [24]. Meanwhile, the operation of the modified-SCAN component of the G-SCAN decoder on the basis of the factor graph is exemplified in Figure 3b.

More specifically, the factor graph of the modified-SCAN algorithm takes the *a-priori* LLRs $\tilde{\mathbf{L}}_a^N$ and *a-priori* LLRs $\tilde{\mathbf{R}}_a^N$ as its input, similarly to the SCAN algorithm [9]. Here, each of the *a-priori* LLRs $\tilde{L}_{i,j}^N$ is initialized to the LLR value provided by the SISO detector, while each of the *a-priori* LLRs $\tilde{R}_{i,j}^N$ is initialized depending on the frozen bit pattern, where an infinity-valued LLR is adopted if the i^{th} one is a frozen bit, and zero-valued LLR is adopted if the i^{th} one is an information bit, where $1 \leq i \leq N$ and $1 \leq j \leq n+1$ represent the index of the bit. Additionally, as mentioned above, the modified-SCAN algorithm also takes a block of bits $\hat{\mathbf{a}}^A$ as its input from the left-hand side, where each bit $\hat{a}_{i,j}^A$ is initialised depending on the bit pattern, so that a zero-valued bit is adopted if the i^{th} is a frozen bit, and the value of the bit provided by the SCL decoder is adopted, if the i^{th} is an information bit.

Within the SCL decoder block and the modified-SCAN decoder block of Figure 2, the internal operations are performed as it will be detailed below. More specifically, the SCL decoder used in step one of the G-SCAN algorithm uses the conventional schedule of the SCL algorithm, which is based on the SC algorithm detailed in [21]. Similarly, the modified-SCAN decoder used in the second step of the G-SCAN algorithm adopts the same schedule as the conventional SCAN algorithm, which is also based on the SC algorithm. More specifically, the SC algorithm can be represented as detailed in [23], where a binary tree having n layers and $N = 2^n$ leaf nodes, there are $2(2N - 2)$ node-visits. This schedule of visiting the nodes is exemplified on a factor graph in Figure 3b, where the steps of the modified-SCAN algorithm are indicated by the step indices in brackets for the case of $N = 8$. More explicitly, the SC schedule starts with the right-to-left propagation of LLRs in step (0), which takes eight channel LLRs as its inputs and appropriately combines them to calculate four LLRs, which are indicated in step (1).

Then, these four LLRs are further combined to obtain two LLRs in step (2). Then, a further combination is performed to obtain one LLR at step (3). After reaching the left-most node in step (3), a left-to-right propagation of LLRs begins in step (4), where the frozen and information LLRs provided on the left-hand edge of the factor graph are taken as input. In step (5) of the SC schedule the operations will be changed right-to-left direction in order to obtain the corresponding LLR. Once the process reached the other left-most node, the process turns again left-to-right propagation with step (6) before obtaining two LLRs in step (7) of Figure 3b. These right-to-left and left-to-right steps are repeated until we reach step (29) of Figure 3b. After this, one inner iteration round can be considered as completed for the modified-SCAN algorithm. If desired, steps (1) to (29) of Figure 3b can be further repeated until reaching the maximum affordable number of iterations (I_{max_i}). Upon completing the final iteration a vector of N extrinsic LLRs may be obtained at the right-hand edge of the factor graph, which can be then passed to the inner detector, as shown in Figure 1. For further details on the scheduling of the SC algorithm, see for example [25].

During the schedule described above, the unit factor graphs generate output LLRs, where different operations are performed at different times during the schedule depending on the availability of input LLRs. The corresponding unit factor graph operations of the modified-SCAN decoder are illustrated in Table IV, where they are compared to the corresponding operations of the SCL and the SCAN algorithms. In Table IV dashed line arrows are used to indicate which output is generated, while solid line arrows used to indicate the inputs, where the selection of particular operations at particular points in the schedule is dictated by the availability of inputs and the outputs. More specifically, there are three types of computations that can be performed by a particular unit factor graph, namely the f function, g function and XOR operation. The f and g functions may be defined as follows, where X and Y represent LLR values and a represents a bit value;

$$f(X, Y) = 2 \tanh^{-1} \left(\tanh \left(\frac{X}{2} \right) \tanh \left(\frac{Y}{2} \right) \right) \quad (1)$$

$$= \text{sign}(X) \text{sign}(Y) \min(|X|, |Y|) + \quad (1a)$$

$$\log \left(1 + e^{-|X+Y|} \right) - \log \left(1 + e^{-|X-Y|} \right) \quad (1a)$$

$$\approx \text{sign}(X) \text{sign}(Y) \min(|X|, |Y|), \quad (1b)$$

$$g(X, Y, a) = (-1)^a X + Y. \quad (2)$$

Here, Eq. (1) and Eq. (1a) represent the exact computation of the f function, while Eq. (1b) is referred to as the min-sum approximation. In practice, using the min-sum approximation typically imposes only small degradation on the BLER performance, while significantly reducing the complexity due to avoiding the calculation of logarithmic and exponential terms.

Note that in Section V, the complexity of each unit factor graph operation of the SCL algorithm will be considered to be a single complexity unit, except for the XOR operation, which will be considered to be zero complexity, since an XOR circuit has a much lower complexity than an adder. However, in the SCAN algorithm, the complexity contribution of each

TABLE III
SUMMARY OF CONTRIBUTIONS OF THE STATE-OF-THE-ART POLAR DECODERS, AS WELL AS WITH EXISTING SURVEYS

Polar decoders	Contribution	Error correction performance	Output information	Complexity
SC [11]	Low complexity polar decoder algorithm.	Weak	Hard	Very low
SCL [10]	Improved error correction performance with cost of L times complexity.	Strong	Hard	Medium
CA-SCL [12]	Improved error detection and correction performance with the aid of CRC bits.	Very strong	Hard	Low
BP [8]	Provides soft outputs with a parallel processing structure. However, an excessive computation complexity memory is required.	Worse than SCL	Soft	High
BPL [13]	Offers a multiple permuted factor graph-based iterative decoding algorithm for polar codes which achieves the same BLER performance as SCL at the cost of complexity.	Same as SCL	Soft	Very high
CA-BPL [14]	Offers close error-rate performance to the CA-SCL decoder.	Close to CA-SCL	Soft	High
SCAN [9]	Provides soft output and requires fewer iteration than BP algorithm.	Worse than SCL	Soft	Medium
Soft-list [15]	Offers a heuristic solution combining a SCL decoder with a BP decoder to improve BLER performance.	Better than SCL	Hard and soft	Medium
The proposed G-SCAN	We propose analytically motivated soft-input soft-output list polar decoding algorithm, which has superior performance than state-of-the-art hard decision SCL decoder.	Better than SCL	Hard and soft	Medium
The proposed CA-G-SCAN	In order to reduce the complexity of the proposed G-SCAN algorithm, a novel CRC-aided G-SCAN algorithm is also proposed, which enables early termination and improves BLER performance.	Better than CA-SCL	Hard and soft	Low

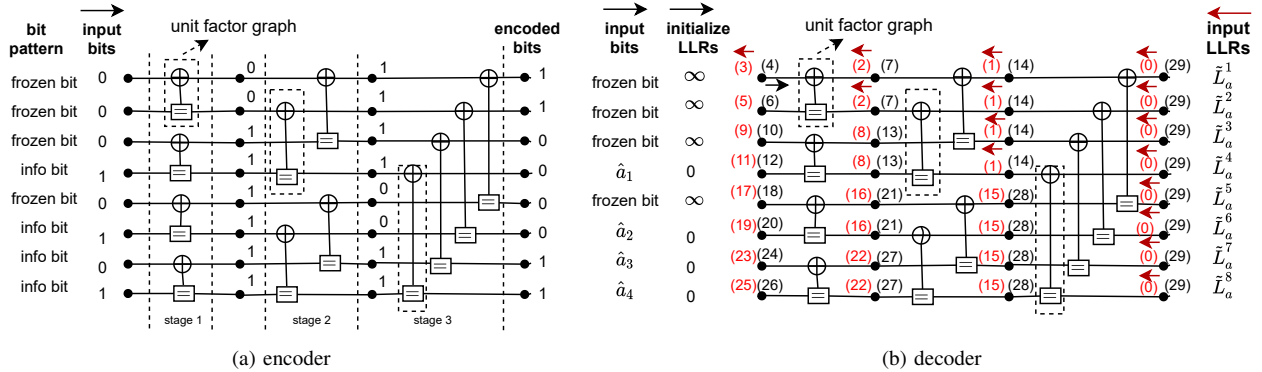


Fig. 3. Figure 3a represents factor graph of polar encoder for the example of converting $A = 4$ information bits [1101] into $N = 8$ encoded bits [11000011], and Figure 3b shows step by step schedule of the proposed modified-SCAN decoder, where bit decision is referred to as \hat{a} , and N number of encoded a -priori LLRs is referred to as \tilde{L}_a^N on the factor graph.

unit factor graph operation will be considered to be of two units, because in addition to the f function they also perform an addition operation. For this reason we refer to these operations as an f^+ function.

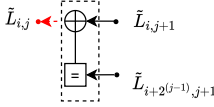
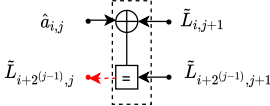
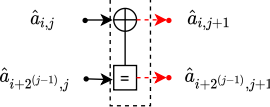
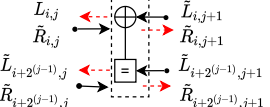
As shown in Table IV, the modified-SCAN algorithm replaces one of the equations used in the conventional SCAN algorithm with an equation from the SCL algorithm. More specifically, one of the double-complexity f^+ function of the SCAN algorithm is replaced by a single-complexity g function inherited from the SCL algorithm. This exchange is motivated by the use of hard-decisions from the SCL algorithm during the modified SCAN algorithm. It is this specific use of the g function in the modified-SCAN algorithm inspired by the SCL hard-decisions that motivates the ‘G’ qualifier in our proposed G-SCAN polar decoder. During the modified-SCAN algorithm, each unit factor graph is processed using one of the

equations selected from Table IV, depending on the availability of LLRs provided on the connections at the right-hand side, as well as upon the availability of LLRs or bits provided on the connections at the left-hand side.

Referring back to the example of Figure 3b, the schedule of the proposed modified-SCAN algorithm starts with the input of LLRs in step (0) at the right hand-edge of the factor graph. Following this, Eq.(4) is used for implementing the right-to-left propagation of LLRs and it is used four times in step (1), two times in step (2), and once in step (3) for producing an uncoded extrinsic LLR at the top left-hand side of the factor graph of Figure 3b. After reaching this top-left node in step (3), a left-to-right propagation is performed in step (4), where the LLRs corresponding to the frozen bit or to the information bit provided at the left-hand edge of the factor graph are taken as input. In step (5) of the schedule seen in Figure 3b,

TABLE IV

THE CORRESPONDING PARTICULAR UNIT FACTOR GRAPH OPERATIONS FOR THE SCL, SCAN, AND G-SCAN DECODERS, WHERE BIT DECISION IS REFERRED AS $\hat{a}_{i,j}$, AND $\tilde{L}_{i,j}$, $\tilde{R}_{i,j}$ ARE LLR MESSAGES WHICH ARE PASSED TO THE LEFT AND RIGHT DIRECTIONS OF THE FACTOR GRAPH, RESPECTIVELY.

Operation	Unit factor graph operation	Equations	Decoders		
			SCL	SCAN	G-SCAN
f function		$\tilde{L}_{i,j} = f(\tilde{L}_{i,j+1}, \tilde{L}_{i+2^{j-1},j+1})$ Eq.(1)	✓	-	✓
g function		$\tilde{L}_{i+2^{j-1},j+1} = g(\tilde{L}_{i,j+1}, \tilde{L}_{i+2^{j-1},j+1}, \hat{a}_{i,j})$ Eq.(2)	✓	-	✓
XOR operation		$\hat{a}_{i,j+1} = XOR(\hat{a}_{i,j}, \hat{a}_{i+2^{j-1},j})$ Eq.(3a)	✓	-	✓
		$\hat{a}_{i+2^{j-1},j+1} = \hat{a}_{i+2^{j-1},j}$ Eq.(3b)	✓	-	✓
f^+ function		$\tilde{L}_{i,j} = f(\tilde{L}_{i,j+1}, [\tilde{L}_{i+2^{j-1},j+1} + \tilde{R}_{i+2^{j-1},j}])$ Eq.(4)	-	✓	✓
		$\tilde{L}_{i+2^{j-1},j} = f(\tilde{L}_{i,j+1}, \tilde{R}_{i,j}) + \tilde{L}_{i+2^{j-1},j+1}$ Eq.(5)	-	✓	-
		$\tilde{R}_{i,j+1} = f(\tilde{R}_{i,j}, [\tilde{R}_{i+2^{j-1},j+1} + \tilde{L}_{i+2^{j-1},j+1}])$ Eq.(6)	-	✓	✓
		$\tilde{R}_{i+2^{j-1},j+1} = f(\tilde{L}_{i,j+1}, \tilde{R}_{i,j}) + \tilde{R}_{i+2^{j-1},j+1}$ Eq.(7)	-	✓	✓

we promptly refer back to the right-to-left propagation, using Eq.(2) to produce an LLR at the left-hand edge. Since we have again reached the left-hand edge of the factor graph, the process again switches to the left-to-right propagation of LLRs in step (6) where the LLRs or the bits provided at the left-hand edge of the factor graph are taken as input. In step (7) of Figure 3b, Eq.(6) and Eq.(7) of Table IV are used for obtaining a pair of LLRs during the left-to-right propagation, as well as Eq.(3) is used for obtaining a pair of bits during the left-to-right propagation. Following this, the schedule progressed step (8) to step (29) of Figure 3b using equations Eq.(2), Eq.(3), Eq.(4), Eq.(6), and Eq.(7) of Table IV in order to produce the final output LLRs at the right-hand edge of the factor graph of Figure 3b.

In summary, by evaluating those equations of Table IV, according to the prescribed SC schedule an LLR may be obtained for each of the N connections at both the left-hand side and the right-hand side of the G-SCAN polar decoder. As described above, the right-hand side output of the modified-SCAN decoder inside the G-SCAN decoder can provide extrinsic feedback LLRs for iteratively decoded schemes, such as the turbo-detected MIMO systems of Figure 1.

B. CRC-aided G-SCAN Polar Decoder Algorithm

As a complement to polar codes used in the control channels of 3GPP 5G NR [22], CRC calculation and attachment is defined. More explicitly, these CRC bits can be used to perform error detection as usual, as well as to aid the correction of 5G NR polar codes. More specifically, the SCL decoder produces

L candidates for the decoded bit sequence and the CRC bits of each candidate can be checked in order to reject any candidate failing the CRC. Then, among the remaining candidates the one having the highest path metric (PM) may be selected to provide the required A number of decoded information bits. In the case where a list size of $L = 8$ is used for SCL decoding, we have to use $\log_2(L = 8) = 3$ of the CRC bits for aiding error correction [22], with the remaining CRC bits used for error detection. On the other hand, if the CRC's of all L decoding candidates have failed, then the decoding process declares a failure. Note that, because we perform L number of CRC checks, we increase the probability of false alarm, which is where a successful CRC check is obtained even though the decoded bits are erroneous. More specifically, the prevalence of this effect is characterised by the False Alarm Rate (FAR) ¹, where the theoretical FAR is given by $2^{-(P-\log_2(L))}$ [22], when P represents the number of CRC bits.

As shown in Figure 4, we have proposed a novel CA-G-SCAN algorithm, in order to facilitate not only error correction and error detection as described above, but also to facilitate an early termination during iterative exchange of extrinsic LLRs between the polar decoder and the concatenated inner detector. More specifically, if a passing CRC is obtained during the SCL decoding then we can terminate the iterative processing and declare success without the need perform further iteration of modified-SCAN algorithm and the concatenated inner detector.

¹In the 3GPP 5G NR standard the FAR is defined as the fraction of erroneously decoded blocks that nonetheless have a passing CRC, in other words "missed detection of an error event" [16], [22].

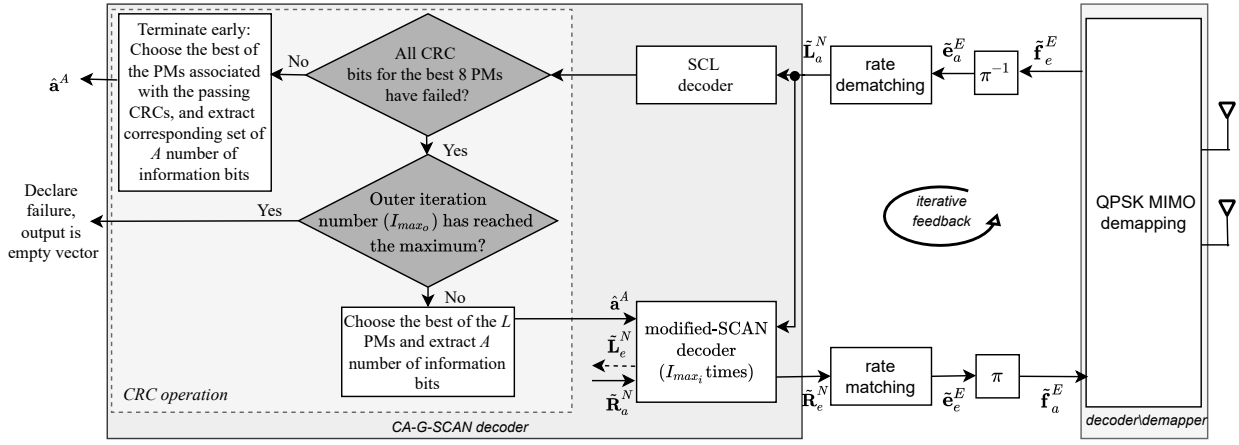


Fig. 4. Basic architecture of the proposed CA-G-SCAN scheme.

By eliminating the operation of modified-SCAN algorithm and turbo-detection steps we achieve significant complexity reduction, as it will be detailed in Section V. However, if the CRC of all L decoding candidates have failed then the decoding candidate having the best PM is chosen to provide A number of information bits, which together with $N - A$ frozen bits are inserted in the modified-SCAN decoder. The modified-SCAN decoder then processes these information bits together with the same block of N encoded *a-priori* LLRs that we provided to the SCL decoder, as described before in Section II-A. This process continues until reaching the maximum outer iteration number I_{max_o} , or until a passing CRC is obtained and early termination is activated. As shown in Figure 4, in the scenario where the maximum number I_{max_o} of outer iterations is reached, the algorithm declares a failure instead of outputting A number of decoded information bits.

III. AN EXAMPLE APPLICATION

This section introduces an example application for the proposed G-SCAN and CA-G-SCAN algorithms, which comprises a turbo-detected 2x2 MIMO system. Following this, in Sections IV, V and VI we will characterise G-SCAN and CA-G-SCAN algorithms in the context of this example application, in terms of their EXIT chart analysis, computational complexity, and error correction and error detection performance, respectively.

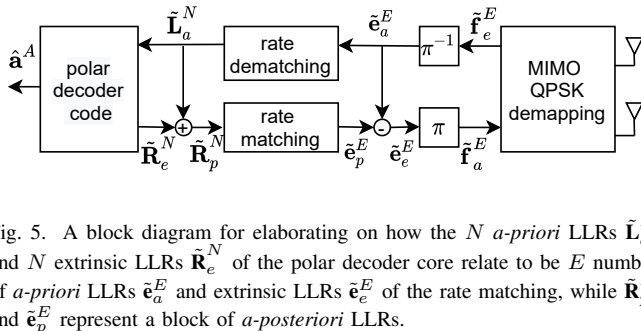


Fig. 5. A block diagram for elaborating on how the N *a-priori* LLRs \tilde{L}_a^N and N extrinsic LLRs \tilde{R}_e^N of the polar decoder core relate to be E number of *a-priori* LLRs \tilde{e}_a^E and extrinsic LLRs \tilde{e}_e^E of the rate matching, while \tilde{R}_p^N and \tilde{e}_p^E represent a block of *a-posteriori* LLRs.

More specifically, in Figure 1 two-stage serially concatenated a polar decoder and a MIMO detector was previously

illustrated, where they iteratively exchanging extrinsic information. Here, the Gray mapped 2x2 QPSK MIMO is used for communication over an uncorrelated narrowband Rayleigh fading channel, where perfect channel knowledge is assumed at the receiver, with no feedback to the transmitter. Here, the spatial multiplexing is employed for the 2x2 MIMO detection to subdivide the data streams into two independent sub-streams for each transmit antenna, rather than for space-time block coding [26]. Furthermore, a Maximum-Likelihood (ML) QPSK MIMO detector [27] is used for the sake of casting the spotlight on the polar decoder.

In addition to the MIMO detector and the polar decoder, our system model also comprises rate matching and dematching components, in order to support flexible coding block lengths as required by the control channels of 3GPP NR [22]. More specifically, in the transmitter, rate matching is employed for adjusting the length of the polar encoded bit sequence from N to E bits, where E represents the encoded block length. In the case of $E < N$, puncturing or shortening is applied, while repetition is applied of $E \geq N$ [22].

A detailed view of the receiver is shown in Figure 5, which illustrates how rate dematching is applied after MIMO detection and deinterleaving (π^{-1}), in order to adjust the length of the *a-priori* LLR block from E to N . More specifically, in the case of repetition, the LLRs of the replicas of each bit in the sequence may be accumulated, in order to obtain a corresponding sequence of N LLRs [22]. By contrast, puncturing refers to the non-transmission of some encoded bits, so the values of these bits are unknown at the receiver [22]. In this case, the corresponding LLRs can be set to zero, followed by interleaving to the set of E received LLRs, in order to obtain the sequence of N LLRs [22]. Meanwhile, shortening involves the non-transmission of coded bits that are guaranteed to have values of zero. In this case, the corresponding LLRs can be set to infinity, followed by interleaving to the set of E received LLRs [22], in order to obtain the sequence of N LLR.

After the rate-dematching of Figure 5, the polar decoder takes these N *a-priori* LLRs as its input and generates N extrinsic LLRs as its output. In order to facilitate turbo-

detection, rate matching is applied for converting these N extrinsic LLRs into a sequence of E extrinsic LLRs. More explicitly, in the case of repetition rate matching in Figure 5 an addition of N *a-priori* LLRs to the N extrinsic LLRs is used for obtaining N *a-posteriori* LLRs, which is the input of the rate matching block. In the case of rate matching extrinsic LLRs we have E number of *a-posteriori* LLRs at the output. Following this, the E number of *a-priori* LLRs are subtracted from these E number of *a-posteriori* LLRs, in order to produce E number of extrinsic LLRs, which are interleaved (π) and then entered into the MIMO detector as its *a-priori* LLRs. In the case of puncturing or shortening, the rate matching block removes a corresponding set of *a-posteriori* LLRs according to puncturing or shortening pattern. In this way, the MIMO detector and polar decoder iteratively exchange their extrinsic LLRs that become *a-priori* LLRs as the input of the other.

All simulations adopted conventional soft-decision output BP and SCAN algorithms benchmarks, which facilitate iterative turbo-detection with the 2x2 MIMO detector. The maximum number of inner iterations performed inside the BP and SCAN algorithms is specified by I_{max_i} , while the maximum number of outer iterations between the polar decoder and the MIMO detector is specified by I_{max_o} . In order to compare different number of inner and outer iterations we adopted the (I_{max_i}, I_{max_o}) notation, which have been used after the name of each decoding technique. For example, BP (1,6) represents a maximum of $I_{max_i} = 1$ inner iteration within the BP decoder, as well as a maximum of $I_{max_o} = 6$ outer iterations between the BP polar decoder and the MIMO detector. Additionally, we adopted a conventional non-turbo SCL decoder having various list sizes L as a hard-decision benchmark. Since there is no turbo-detection, this SCL decoding benchmark only benefits from one-shot MIMO detection, as mentioned before.

Furthermore, in addition to the SCAN and BP benchmarks described above, we also proposed a pair of novel hybrid algorithms, which we refer to as the SCAN-SCL and BP-SCL decoders. In both of these algorithms, the SCAN and BP algorithms are activated as usual during the initial turbo-detection iterations, but in the final turbo-detection iteration upon reaching the iteration limit I_{max_o} , these novel benchmarks activate the SCL algorithm using a particular list size L . In this way, these novel benchmarks benefit from superior hard-decision performance.

IV. EXTRINSIC INFORMATION TRANSFER CHART ANALYSIS

This section characterises the EXIT chart analysis of the G-SCAN algorithm in the context of the example application from Section III.

The EXIT chart analysis is a useful tool for visually characterizing the proposed system, as well as for verifying the operation of the proposed algorithm [28]–[30]. As illustrated in Figure 6, the EXIT functions of the 2x2 QPSK MIMO detector as well as the SCAN and G-SCAN polar decoders are characterized using two different methods of measuring mutual information (MI), namely the information averaging method and the histogram based method [31]. The information

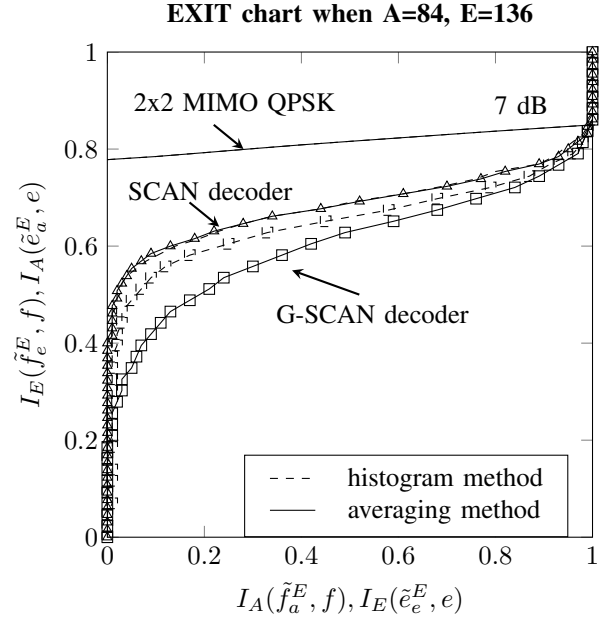


Fig. 6. The EXIT charts of the 2x2 QPSK MIMO detector, as well as the SCAN and G-SCAN decoders, where each using both averaging and histogram methods for measuring mutual information. Here, an information block length of $A = 84$, and an encoded block length of $E = 136$ are used when $I_{max_i} = 1$ and $L = 2$ for communication over a Rayleigh fading channel.

averaging method estimates the quality of LLRs by considering only their magnitude. By contrast, the histogram based method characterizes the quality of the iteratively exchanged LLRs by comparing them to the corresponding bits. Here, the information averaging method makes the assumption that the LLRs are trustworthy, while the histogram method does not trust the LLRs, hence it compares them to the corresponding hard-decision bit values. In this way, if there is a good match between these two methods, this indicates that the LLRs are indeed trustworthy, and hence verifies bit-suggestion of the proposed scheme. As illustrated in Figure 6, the SCAN decoder and 2x2 MIMO detector have a perfect match between the averaging and histogram methods, confirming their bit-suggestion. By contrast, the G-SCAN decoder exhibits a small gap between these two methods, which may be explained by hard-decisions which are made inside the G-SCAN algorithm. These hard-decisions impose maximum confidence rightly or wrongly upon some of the decisions made by the decoder, which occasionally represent the over-confidence of the LLRs. However, as our BLER results will show, although some LLRs produced by the G-SCAN may indeed be over-confident, this does not translate into performance degradation. We surmise that the over-confidence of the LLRs output by the G-SCAN decoder does not prevent it from outperforming the SCAN decoder, because Figure 6 shows that the EXIT chart tunnel created using the histogram based method is wider for the G-SCAN decoder than for the SCAN decoder. Indeed it is the histogram based method of measuring the mutual information, which characterises the true quality of the LLRs.

Section VI will show that the G-SCAN algorithm provides better performance than the SCAN algorithm. As shown in

Figure 7, the gap between the averaging and histogram based methods when plotting the EXIT function of the G-SCAN decoder reduces, as the encoded block length increases and as we shift from shortening to repetition for rate matching. Nonetheless, our future work will consider techniques for applying transformations to the LLRs produced by the G-SCAN algorithm in order to reduce any over-confidence to yield a good match between the averaging and histogram methods.

As shown in Figure 7, the proposed G-SCAN algorithm may be further validated by measuring the mutual information during the real iterative turbo-detection process, and plotting the results in trajectories between the EXIT functions of the polar decoder and the 2x2 MIMO detector. Figure 7 shows that, for each rate matching mode considered the corner points of the stair-case-shaped real decoding trajectory are in close agreement with the EXIT functions, particularly those of the averaging method, which validates our analysis of these EXIT functions.

Figure 8 compares the EXIT function of the SCAN and G-SCAN decoders for each rate matching mode using an information averaging method. Additionally, Figure 8 shows the EXIT function of the 2x2 QPSK MIMO detector over a range of SNR values aligning from -2 dB to 8 dB. If the EXIT function of the polar decoder does not intersect that of the MIMO detector before reaching the right-hand edge of the EXIT chart, where $I_A = 1$, then the EXIT chart tunnel between the MI curves of the inner and outer decoder can be considered to be open and hence a low block error rate may be expected [29]. By contrast, if they do intersect before the right-hand edge, then the EXIT chart tunnel is considered to be closed and high block error rate may be expected.

To elaborate further, in the case of closed tunnel a lower BLER may be expected if the intersection point is further to the right-hand edge of the EXIT chart. For example, in the case of using the repetition mode at 0 dB, the EXIT curve of the SCAN decoder intersects that of the 2x2 QPSK MIMO detector at $I_A = 0.82$, whereas the G-SCAN decoder intersects at $I_A = 0.95$. This implies that the G-SCAN decoder will exhibit a lower BLER than the SCAN decoder in the case of repetition at 0 dB, as it will be demonstrated in Section VI. More generally, if the area under the EXIT function of the polar decoder is large, then higher SNR would be required in order to create an open EXIT chart tunnel. For example, 2 dB is sufficient to create an open tunnel when we use the repetition ($E = 272$), but 7 dB is required in order to create an open tunnel in the case of shortening ($E = 136$) when $A = 84$, for both the SCAN and G-SCAN decoders.

V. COMPLEXITY ANALYSIS

This section characterises computational complexity of the proposed G-SCAN and CA-G-SCAN algorithms in the context of the example application from Section III, comparing them to the relevant soft- and hard-decision output benchmarks, across a wide variety of different rate matching modes.

In order to find the optimal performance vs. complexity balance, we have compared the proposed G-SCAN algorithm

TABLE V
COMPLEXITY OF CONSIDERED POLAR DECODER ALGORITHMS.

Algorithm	Complexity
SC decoder	$\mathcal{O}(N \log N)$
SCL and CA-SCL decoder	$\mathcal{O}(LN \log N)$
SCAN decoder	$\mathcal{O}(I_{max_i} N \log N)$
BP decoder	$\mathcal{O}(I_{max_i} N \log N)$
SCAN-SCL decoder	$\mathcal{O}(I_{max_i} N \log N) + \mathcal{O}(LN \log N)$
BP-SCL decoder	$\mathcal{O}(I_{max_i} N \log N) + \mathcal{O}(LN \log N)$
G-SCAN and CA-G-SCAN decoder	$\mathcal{O}(LN \log N) + \mathcal{O}(I_{max_i} N \log N)$

and its benchmarks in this section. Table V provides our complexity equations of the polar decoders considered and the associated performance will be investigated in Section VI. As shown in Table V, the SC algorithm has the lowest complexity among all the polar decoders considered [10]. However, it is well known the SC algorithm suffers from weak BLER performance. On the other hand, the SCL algorithm provides much better BLER performance at the cost of having L times higher complexity than the SC algorithm, owing to using a list comprising L candidate paths [10], [24]. Note that $L = 8$ is typical for SCL algorithms, since its performance improves only modestly above this value [24].

In the case of the iterative SCAN and BP algorithms, the complexity mostly depends upon the maximum number of inner iteration performed, which is denoted by I_{max_i} in Table V. Although the SCAN decoding algorithm has the same computational complexity per iteration as the BP decoding algorithm [32], in general the SCAN algorithm has lower complexity than the BP algorithm since it can achieve similar BLER performance using fewer iterations [9], [13], as it will be demonstrated in Section VI.

On the other hand, the complexity of proposed novel SCAN-SCL and BP-SCL hybrid algorithms depends not only on the maximum number I_{max_i} inner iterations performed, but also upon the list size L . More explicitly, their complexity may be computed as the complexity of the conventional SCAN or BP algorithm plus the complexity of the SCL algorithm, as illustrated in Table V. Note that, despite giving better BLER performance than the conventional BP algorithm, the hybrid BP-SCL algorithm also benefits from lower complexity, since it requires fewer inner iteration than the conventional BP algorithm for achieving a similar performance, as it will be demonstrated in Section VI. As far the proposed G-SCAN algorithm, its complexity is also based mainly on the list size L and on the maximum number of inner iterations performed within the modified-SCAN algorithm, since the first step in each iteration comprises the operation of the SCL algorithm, with a second step comprising that of the modified-SCAN algorithm. In particular, we will show that performing only one inner iteration $I_{max_i} = 1$ for the G-SCAN scheme is sufficient to outperform various benchmarks. Hence, its complexity may also be represented by $\mathcal{O}(LN \log N) + \mathcal{O}(N \log N)$.

In order to make a more detailed comparison, Table VI compares the computational complexity of the algorithms considered, in terms of the number of Add Compare Select (ACS)

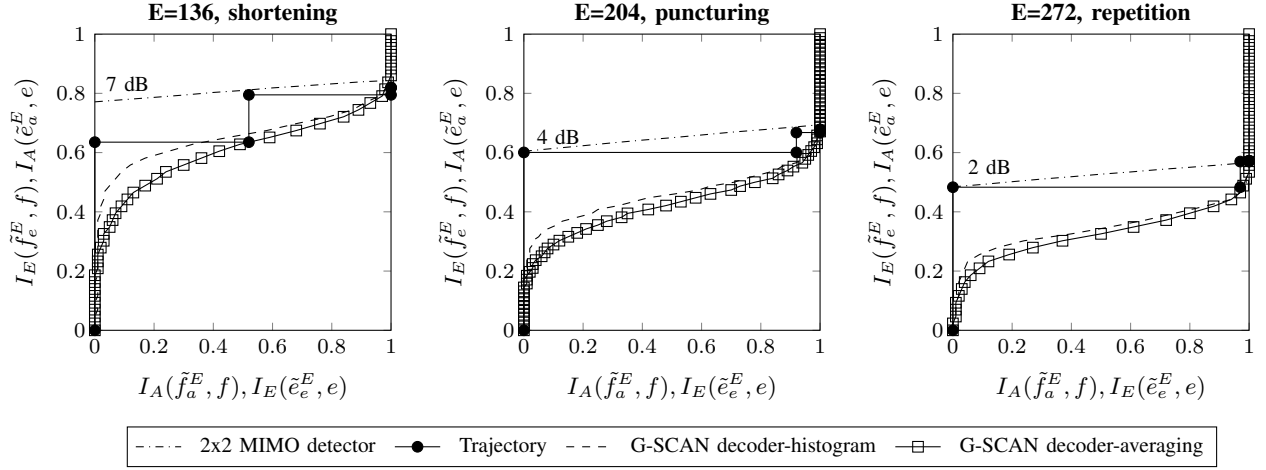


Fig. 7. Plots of EXIT functions and the trajectories in the proposed G-SCAN decoder for each rate matching mode, when $A = 84$, $I_{max_i} = 1$ and $L = 2$.

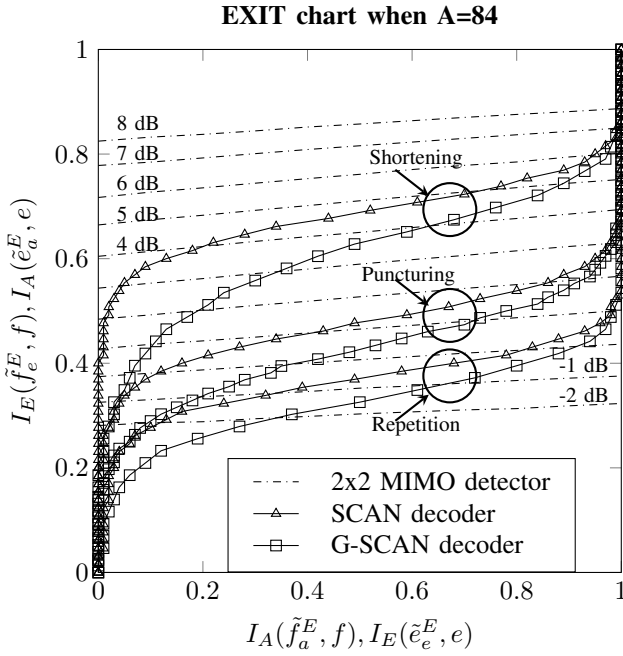


Fig. 8. EXIT functions of the G-SCAN and SCAN polar decoders, as well as the EXIT function of the 2x2 MIMO QPSK detector, for the case of performing $I_{max_i} = 1$, $L = 2$, using an information block length of $A = 84$, and encoded block lengths of $E = 272$ for repetition, $E = 204$ for puncturing and $E = 136$ for shortening, in the case of communication over a Rayleigh fading channel.

operations performed, both for the short block lengths having $A = 84$ bits, as well as for the longer block lengths comprising $A = 336$ bits. More specifically, with reference to Table IV, the total number of each f , g and f^+ operation performed by each polar decoder is calculated, for various values of L , I_{max_i} and I_{max_o} . Note that the specific choice of each L , I_{max_i} and I_{max_o} value given in Table VI will be justified in Section VI. Note that the complexity results of Table VI for the G-SCAN decoder can also be considered to set an upper bound on the complexity of the corresponding CA-G-

TABLE VI
COMPUTATIONAL COMPLEXITY ANALYSIS OF POLAR DECODER ALGORITHMS

	L	I_{max_i}	I_{max_o}	Complexity	
				$A = 84$ $E = 136$ $N = 256$	$A = 336$ $E = 1084$ $N = 1024$
SC	1	-	-	2,388	20,816
SCL and CA-SCL	2	-	-	4,132	28,272
	4	-	-	7,524	43,144
	8	-	-	14,228	72,856
	16	-	-	27,572	132,256
	32	-	-	56,004	251,040
SCAN	-	1	4	32,768	163,840
	-	1	10	81,920	409,600
	-	2	4	65,536	327,680
	-	2	10	163,840	819,200
SCAN-SCL	2	1	4	36,900	192,112
	2	1	10	86,052	437,872
BP	-	1	4	32,768	163,840
	-	10	4	327,680	1,638,400
	-	10	10	819,200	4,096,000
BP-SCL	2	1	4	36,900	192,112
	2	10	4	331,820	1,666,672
	2	1	10	82,333	412,427
	2	10	10	823,332	4,124,272
	2	1	4	45,200	256,448
G-SCAN and upper bound CA-G-SCAN	2	1	10	113,000	641,120
	4	1	4	58,768	315,936
	4	1	10	146,920	789,840
	8	1	4	85,584	434,784
	8	1	10	213,960	1,086,960

SCAN decoder. More specifically, in the case of successful decoding relying on early termination, the complexity will be lower than the quoted values of Table VI. By contrast, in the case of unsuccessful decoding, no early termination will be possible and hence the full complexity provided in Table VI will be incurred.

In the case of short block lengths where $A = 84$ and $E = 136$, Table VI reveals that the proposed G-SCAN(1, 4, $L = 2$) algorithm has 30% lower complexity than the SCAN(2, 4)

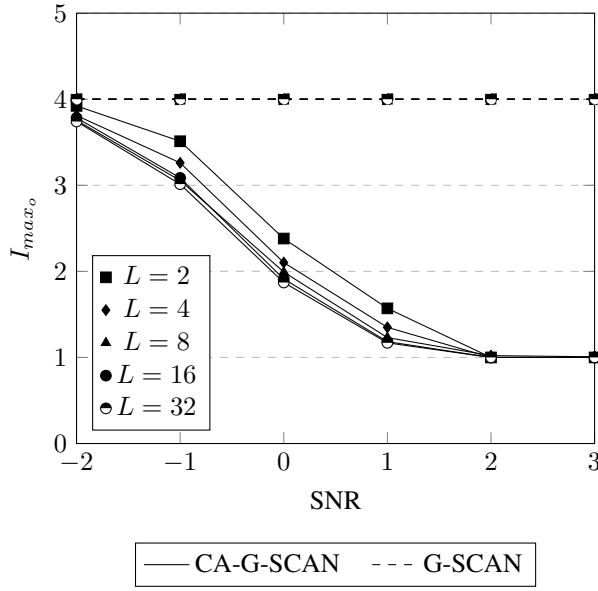


Fig. 9. Average number of outer iterations I_{max_o} performed by the proposed G-SCAN and CA-G-SCAN algorithms, when an information block length of $A = 84$, and an encoded block length of $E = 272$ is used in the case of communication over a 2x2 QPSK MIMO Rayleigh fading channel.

benchmark, as well as having the benefit of offering superior BLER performance, as the analysis of Section VI will show. In the case of longer blocks of $A = 336$ and $E = 1084$, the proposed G-SCAN(1, 10, $L = 2$) algorithm has approximately 20% lower complexity than the SCAN(2, 10) benchmark, as well as also offering the benefit of superior BLER performance. Likewise, the analysis of Section VI will show that the proposed G-SCAN algorithm having a low list size of $L = 2$ and performing only $I_{max_i} = 1$ inner iterations offers superior BLER performance over an SCL decoder having the list size of $L = 32$. In this case, Table VI shows that proposed G-SCAN algorithm has approximately 20% lower complexity than this SCL benchmark in the case of short blocks. On the other hand, for longer blocks the complexity of the G-SCAN is slightly higher than that of the SCL $L = 32$, but still having the advantage of offering superior BLER performance, as it will be demonstrated in Section VI.

In order to reduce the complexity of the G-SCAN algorithm, an early termination scheme relying on a CRC check was proposed in Section II-B. Here, a CRC check is performed following the SCL decoding during each outer iteration between the MIMO detector and the CA-G-SCAN decoder, where iterative decoding is terminated if the CRC passes. This eliminates the complexity associated with the modified-SCAN step in that corresponding iteration, which has a complexity of $\mathcal{O}(N \log N)$. Furthermore, this also eliminates the complexity associated with performing further outer iterations between the polar decoder and the MIMO detector. Figure 9 shows the average number of outer iterations performed by the proposed G-SCAN and the CA-G-SCAN algorithm, when using an information block length of $A = 84$ bits and an encoded block length of $E = 272$ bits. As expected, Figure 9 shows that increasing the SNR value reduces the number of outer

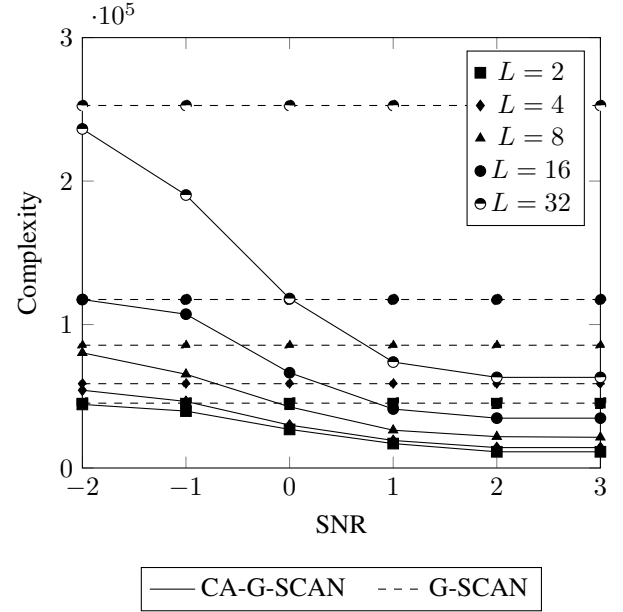


Fig. 10. Complexity of the proposed G-SCAN and CA-G-SCAN algorithms, when an information block length of $A = 84$, and an encoded block length of $E = 272$ is used in the case of communication over a 2x2 QPSK MIMO Rayleigh fading channel.

iterations performed by the CA-G-SCAN algorithm. Additionally, Figure 10 illustrates the corresponding complexity reduction. Furthermore, Table VI shows that the proposed G-SCAN algorithm has a computational complexity of 58,768 operations for $A = 84$, $L = 4$ and $I_{max_o} = 4$. But for the CA-G-SCAN algorithm Figure 10 shows that the complexity is reduced to 14,228 for SNR = 2 dB, which corresponds to 75% complexity reduction.

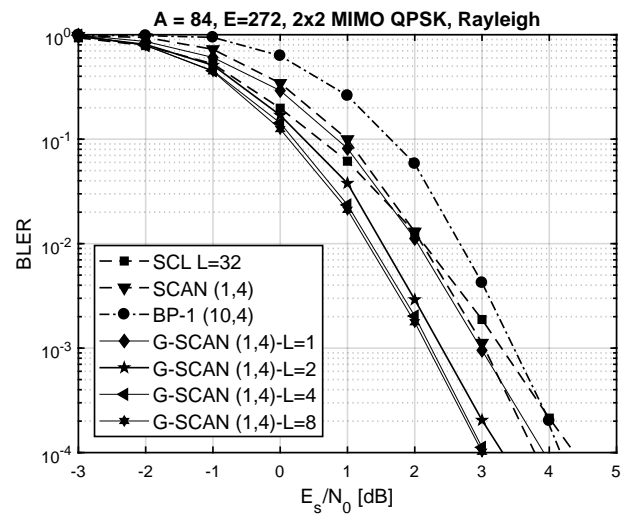


Fig. 11. BLER performance of the proposed G-SCAN decoder with various number of list sizes, for the block lengths of $A = 84$ and $E = 272$, when using 2x2 QPSK MIMO for communication over an uncorrelated narrowband Rayleigh fading channel.

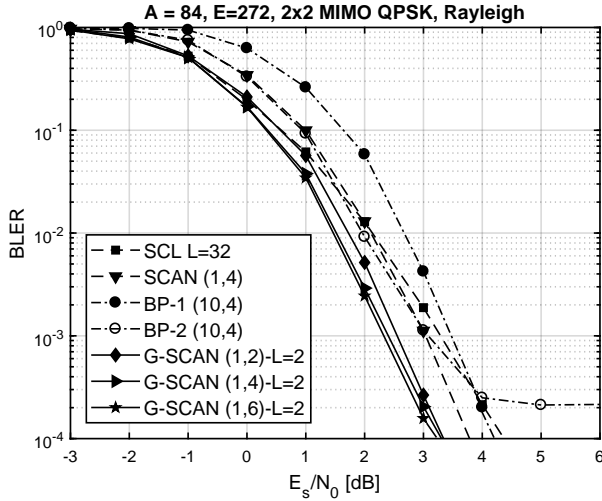


Fig. 12. BLER performance of the proposed G-SCAN decoder when using various numbers of outer iteration (I_{max_o}) for the block lengths of $A = 84$ and $E = 272$, when using 2x2 QPSK MIMO for communication over an uncorrelated narrowband Rayleigh fading channel.

VI. PERFORMANCE ANALYSIS

This section characterises error correction and error detection performance of the proposed G-SCAN and CA-G-SCAN algorithms in the context of the example application from Section III, comparing them to the relevant soft- and hard-decision output benchmarks, across a wide variety of different rate matching modes.

In order to investigate the performance of both the proposed schemes and the benchmarks, the BLER vs. the Signal to Noise Ratio (SNR) E_s/N_0 is quantified for the system model of Figure 1, which employs a 2x2 QPSK MIMO scheme for communication over an uncorrelated narrowband Rayleigh fading channel. In order to investigate the performance for short blocks, an information block length of $A = 84$ is selected, together with encoded block lengths of $E = 272$, $E = 204$ and $E = 136$, which are specially chosen to activate the repetition, puncturing and shortening rate matching modes, respectively. Likewise, to investigate the performance of longer blocks, an information block length of $A = 336$ is considered together with the encoded block lengths of $E = 1084$, $E = 816$ and $E = 544$, for the repetition, puncturing and shortening rate matching modes, respectively. Note that all schemes used the min-sum approximation of Eq. (1b), except for the BP algorithm, which employed both the min-sum approximation and the exact computation, represented by BP-1 and BP-2, respectively.

Figure 11 investigates the impact of various list sizes L upon the BLER performance of the proposed G-SCAN algorithm, when using $I_{max_o} = 4$ outer iterations. These results are compared to the SCL benchmark using a list size of $L = 32$. As it may be expected, Figure 11 shows that the BLER performance improves upon increasing the list size L used by the G-SCAN algorithm. Furthermore, Figure 11 shows that the proposed G-SCAN algorithm offers significant gain over

the SCL benchmark, namely up to 1.5 dB gain at BLER of 10^{-4} . However, the performance improvements become quite modest for higher values of L . For example, increasing the list size from $L = 1$ to $L = 2$ provides almost 0.75 dB gain, while increasing it from $L = 2$ to $L = 4$ provides only 0.25 dB gain. Hence, when the complexity to be detailed in Section V is considered, a list size of $L = 2$ or $L = 4$ may be recommended to strike an attractive trade-off for the G-SCAN algorithm, especially for short blocks.

Note that, Figure 11 also characterises the BLER performance of the iterative SCAN and BP polar decoders, as additional benchmarks. In the case of using $I_{max_o} = 4$ outer iterations, Figure 11 shows that even if the conventional BP-1 algorithm uses $I_{max_i} = 10$ inner iterations, it is outperformed by about 0.5 dB with using the conventional SCAN algorithm employing only $I_{max_i} = 1$ inner iteration. Further to this, using the same number of $I_{max_o} = 4$ outer iterations, the proposed G-SCAN shows even better performance employing only $I_{max_i} = 1$ inner iteration. More specifically, for the block lengths of $A = 84$ and $E = 272$, the G-SCAN algorithm with $L = 4$ offers 1.2 dB gain over BP-1 algorithm, and almost 1 dB gain over the SCAN algorithm, at a BLER of 10^{-4} .

Figure 12 shows that as expected, increasing the number of outer iterations performed by the proposed G-SCAN algorithm improves the performance, owing to the iterative feedback gain of turbo-detection. More specifically, Figure 12 characterises the performance of the proposed G-SCAN algorithm when the number of outer iterations increased from $I_{max_o} = 2$ to $I_{max_o} = 6$, when using a constant list size of $L = 2$. It may be observed that the performance improvements saturate, as the number of outer iterations is increased. For example, increasing the number of outer iteration from $I_{max_o} = 2$ to $I_{max_o} = 6$ provides only 0.3 dB gain, despite having three times higher complexity. Hence, when the complexity of Section V is considered, $I_{max_o} = 4$ may be recommended for striking an attractive trade-off for the G-SCAN algorithm, especially for short blocks.

Note that, in addition to the min-sum approximation of Eq. (1b), Figure 12 shows the performance of the BP algorithm when using the exact computation of Eq. (1a). Here, BP-1 refers to the min-sum approximation, while BP-2 refers to the exact computation. As shown in Figure 12, the exact computation gives better BLER performance than the min-sum approximation, but it suffers from an error floor at higher SNRs. This is because the exact-computation converges more promptly towards a decoding decision, which on occasions may be incorrect. By contrast, the min-sum approximation takes longer to converge, but this approach allows it to avoid incorrect decoding decisions, in the same way as the successive relaxation can benefit iterative decoders. Note that the exact computation of the BP-2 algorithm is associated with the highest complexity among all of the polar decoders considered. Hence, we will only consider the BP-1 algorithm as a benchmark for the rest of the simulations discussed in this section.

Again, rate matching has a significant impact on the performance of the 5G NR polar codes. Therefore, Figure 13 investigates the performance of all polar decoding algorithms

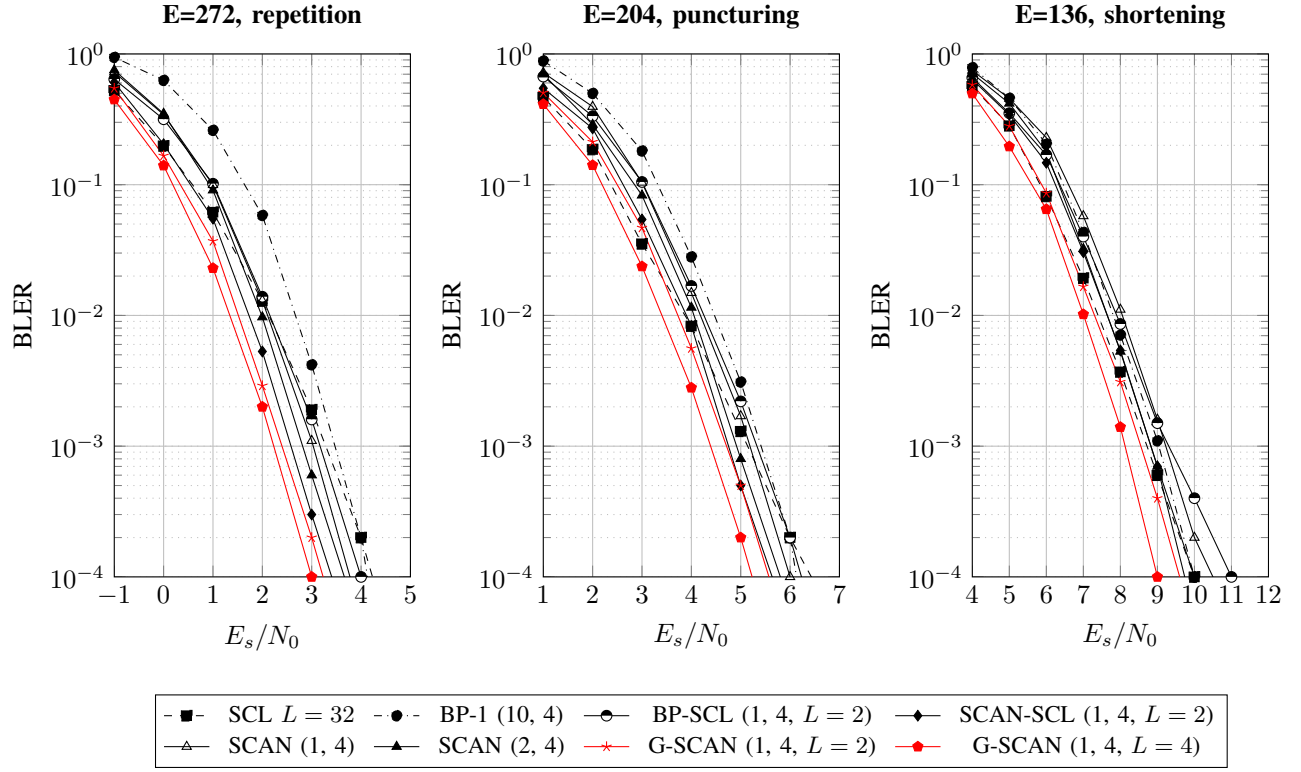


Fig. 13. BLER performance of various different polar decoders when using a short information block length of $A = 84$ bits, for the case of repetition ($E = 272$), puncturing ($E = 204$) and shortening ($E = 136$) rate matching modes, while using 2x2 QPSK MIMO for communication over an uncorrelated narrowband Rayleigh fading channel.

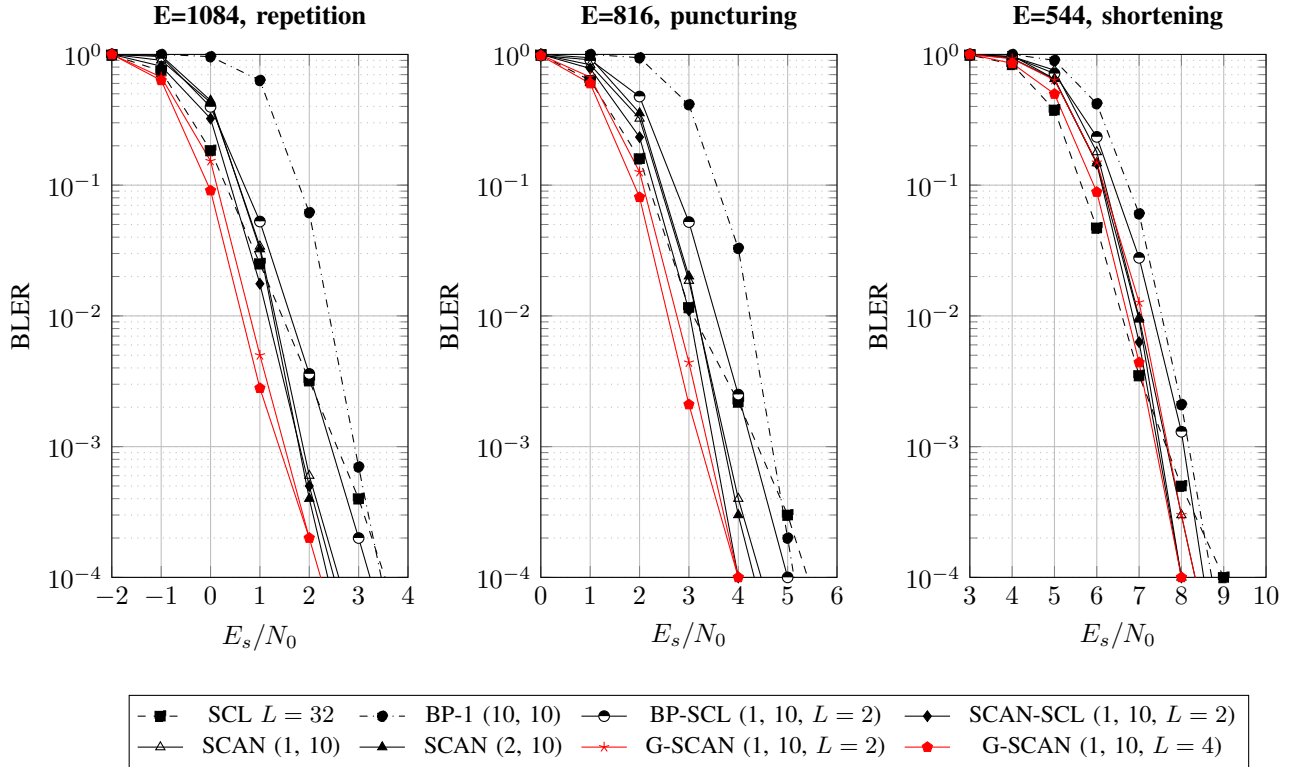


Fig. 14. BLER performance of various different polar decoders when using a long information block length of $A = 336$ bits, for the case of repetition ($E = 1084$), puncturing ($E = 816$) and shortening ($E = 544$) rate matching modes, while using 2x2 QPSK MIMO for communication over an uncorrelated narrowband Rayleigh fading channel.

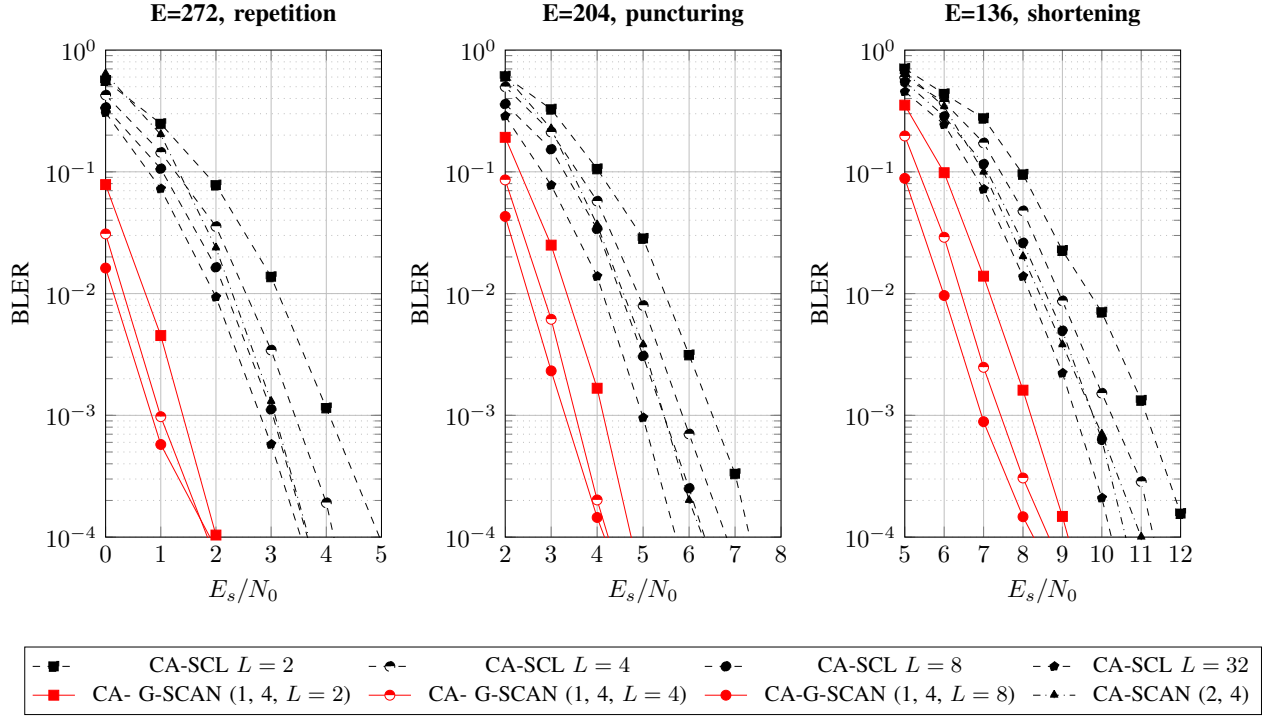


Fig. 15. BLER performance of the proposed CRC-aided G-SCAN algorithm when using an information block length of $A = 84$, for the repetition ($E = 272$), puncturing ($E = 204$) and shortening ($E = 136$) rate matching modes, while using 2x2 QPSK MIMO for communication over an uncorrelated narrowband Rayleigh fading channel.

considered while using different rate matching modes. Figure 13 shows that upon using a short information block length of $A = 84$ bits, the proposed G-SCAN algorithm using $I_{max_i} = 1$ inner iteration, $I_{max_o} = 4$ outer iterations and a list size of $L = 4$ offers superior performance across all rate matching modes. By contrast, the benchmarks typically only perform well for a subset of the rate matching modes. As an example, the BP-1 algorithm is outperformed by the SCAN and the BP-SCL algorithms in the case of the repetition ($E = 272$) and puncturing ($E = 204$) rate matching modes, although at the cost of a higher complexity it becomes capable of better than them in the case of shortening ($E = 136$) mode.

In order to consider the effect of longer information block lengths, Figure 14 characterises the performance of the proposed algorithms and various benchmarks for an information block length of $A = 336$, for the case of each rate matching mode. Similar to case of short blocks, the proposed G-SCAN algorithm using $I_{max_i} = 1$, $I_{max_o} = 10$ and $L = 4$ offers superior performance across all rate matching modes. By contrast, the benchmarks typically only perform well for a subset of the rate matching modes. For example, in the case of the shortening mode, the proposed hybrid SCAN-SCL algorithm using $I_{max_i} = 1$, $L = 2$ performs similarly to the G-SCAN algorithm with $I_{max_i} = 1$, $L = 4$. However, in the case of repetition, the proposed G-SCAN algorithm using either the list size of $L = 2$ or $L = 4$ offers approximately 0.3 dB gain over the hybrid SCAN-SCL algorithm.

As a complement to the BLER plots of Figures 13 and 14, for the proposed G-SCAN algorithm, Figure 15 characterises the BLER plots of proposed CA-G-SCAN algorithm, while

considering list sizes of $L = 2$, $L = 4$ and $L = 8$, for each rate matching mode. As mentioned in Section II-B, the 3GPP 5G NR polar codes adopt an 11-bit CRC for the uplink channels, which is concatenated at the end of the information bits [22]. In the proposed CA-G-SCAN decoder scheme, $\log_2(L)$ of these $P = 11$ CRC bits [22] are used for aiding error correction, while the remaining $[P - \log_2(L)]$ CRC bits are used for error detection, in accordance with the CA-SCL decoding algorithm, as described in Section II-B. In this way, the CA-G-SCAN decoder offers enhanced BLER performance compared to the G-SCAN decoder. In all cases, it may be observed that the CA-G-SCAN algorithm having a list size of $L = 2$ outperforms the CA-SCL benchmark having a list size of $L = 32$. More specifically, the proposed scheme offers more than 1 dB gain, despite having slightly lower complexity, as shown in Table VI when $I_{max_i} = 1$, $I_{max_o} = 4$. Figure 10 shows that the early terminated CA-G-SCAN provide significant complexity reduction without any substantial performance loss over the proposed G-SCAN algorithm.

VII. CONCLUSION

We have recognized and exploited that the conventional turbo-detected soft-in soft-out polar decoders such as the BP and the SCAN algorithms offer poor error correction performance compared to the state-of-the-art hard-decision SCL algorithm. Hence, we have identified a gap in the literature for a SISO polar decoder that has better performance than SCL decoding. This gap motivated us to propose a novel G-SCAN

polar decoding algorithm, which generates not only soft-decision outputs but also hard-decision outputs, combining the hard decision outputs of the SCL decoder and the soft-in soft-out capability of the SCAN decoder.

We have analyzed the EXIT characteristic of the proposed algorithm, as well as its performances and complexity when compared to various hard- and soft-decision polar decoder benchmarks. We have shown that concatenating a 2x2 QPSK MIMO detector with the proposed G-SCAN decoder having a list size of $L = 2$ offers up to 1 dB gain over the state-of-the-art hard-decision SCL decoder using a list size of $L = 32$, across each 3GPP rate matching mode. Furthermore, in order to reduce the complexity of the proposed algorithm, a novel CA-G-SCAN algorithm has also been proposed, which enables early termination and improves BLER performance. In our future work, we will consider higher-order modulation as well as a higher number of transmitter and receiver antennas for MIMO detection, such as 4x4 MIMO with the help of sphere decoding [33], [34].

REFERENCES

- [1] "3GPP TS 21.101, UTRAN-based 3GPP system (Release 9)," Tech. Rep.(TR), May 2010.
- [2] L. Hanzo, T. H. Liew, and B. L. Yeap, *Turbo coding, Turbo Equalisation and Space-Time Coding*. John Wiley & Sons, 2002.
- [3] J. Woodard and L. Hanzo, "Comparative Study of Turbo Decoding Techniques: An overview," *IEEE Trans. Veh. Technol.*, vol. 49, no. 6, pp. 2208–2233, 2000.
- [4] L. Hanzo, J. P. Woodard, and P. Robertson, "Turbo Decoding and Detection for Wireless Applications," *Proc. IEEE*, vol. 95, no. 6, pp. 1178–1200, 2007.
- [5] C. Douillard, M. Jézéquel, C. Berrou, D. Electronique, A. Picart, P. Didier, and A. Glavieux, "Iterative Correction of Intersymbol Interference: Turbo-equalization," *Eur. Trans. Telecommun.*, vol. 6, no. 5, pp. 507–511, 1995.
- [6] C. S. Park, Y. E. Wang, G. Jöngren, and D. Hammarwall, "Evolution of Uplink MIMO for LTE-Advanced," *IEEE Commun. Mag.*, vol. 49, no. 2, pp. 112–121, 2011.
- [7] M. Tüchler and A. C. Singer, "Turbo Equalization: An overview," *IEEE Trans. Inf. Theory*, vol. 57, no. 2, pp. 920–952, 2011.
- [8] Y. Zhang, Q. Zhang, X. Pan, Z. Ye, and C. Gong, "A Simplified Belief Propagation Decoder for Polar Codes," *2014 IEEE Int. Wireless Symp. IWS*, pp. 2–5, 2014.
- [9] U. U. Fayyaz and J. R. Barry, "Low-Complexity Soft-Output Decoding of Polar Codes," *IEEE J. Sel. Areas Commun.*, vol. 32, no. 5, pp. 958–966, 2014.
- [10] I. Tal and A. Vardy, "List Decoding of Polar Codes," *IEEE Trans. Inf. Theory*, vol. 61, no. 5, pp. 2213–2226, 2015.
- [11] E. Arikan, "A Performance Comparison of Polar Codes and Reed-Muller Codes," *IEEE Commun. Lett.*, vol. 12, no. 6, pp. 447–449, 2008.
- [12] K. Niu and K. Chen, "CRC-Aided Decoding of Polar Codes," *IEEE Commun. Lett.*, vol. 16, no. 10, pp. 1668–1671, 2012.
- [13] A. Elkelesh, M. Ebada, S. Cammerer, and S. Ten Brink, "Belief Propagation List Decoding of Polar Codes," *IEEE Commun. Lett.*, vol. 22, no. 8, pp. 1536–1539, 2018.
- [14] M. Geiselhart, A. Elkelesh, M. Ebada, S. Cammerer, and S. t. Brink, "CRC-Aided Belief Propagation List Decoding of Polar Codes," *IEEE Int. Symp. Inf. Theory (ISIT)*, 2020.
- [15] L. Xiang, Y. Liu, Z. B. K. Egilmez, R. G. Maunder, L.-L. Yang, and L. Hanzo, "Soft List Decoding of Polar Codes," *IEEE Trans. Veh. Technol.*, vol. 69, no. 11, pp. 13 921–13 926, 2020.
- [16] "3GPP TS 38.212, 3rd Generation Partnership Project; Tech. Specification Group Radio Access Network; NR; Multiplexing and Channel Coding (Release 15) V15.6.0," Tech. Specification (TS), June 2019.
- [17] D. Hui, S. Sandberg, Y. Blankenship, M. Andersson, and L. Grosjean, "Channel Coding in 5G New Radio: A Tutorial Overview and Performance Comparison with 4G LTE," *IEEE Trans. Veh. Technol.*, vol. 13, no. 4, pp. 60–69, 2018.
- [18] H. Futaki and T. Ohtsuki, "Low-Density Parity-Check (LDPC) Coded MIMO Systems with Iterative Turbo Decoding," in *IEEE 58th Veh. Technol. Conf. VTC 2003-Fall (IEEE Cat. No.03CH37484)*, vol. 1, 2003, pp. 342–346 Vol.1.
- [19] A. Charaf, P. Pénard, L. Cariou, and G. R-Guisantes, "Turbo-equalization of LDPC Coded MIMO Inner/Outer Scheduling," in *Int. Conf. Wireless Comm. Signal Process. (WCSP)*, 2010, pp. 1–5.
- [20] A. Al-Dulaimi, X. Wang, and C.-L. I, "Code Design for Multiuser MIMO," in *5G Networks: Fundamental Requirements, Enabling Technologies, and Operations Management*, 2018, pp. 205–236.
- [21] E. Arikan, "Channel Polarization: A method for Constructing Capacity-Achieving Codes for Symmetric Binary-Input Memoryless Channels," *IEEE Trans. Inf. Theory*, vol. 55, no. 7, pp. 3051–3073, 2009.
- [22] Z. B. K. Egilmez, L. Xiang, R. G. Maunder, and L. Hanzo, "The Development, Operation and Performance of the 5G Polar Codes," *IEEE Commun. Surveys Tut.*, vol. 22, no. 1, pp. 96–122, 2019.
- [23] C. Kestel, S. Weithoffer, and N. Wehn, "Polar Code Decoder Exploration Framework," *Adv. Radio Sci.*, vol. 16, 2018.
- [24] Z. Babar, Z. B. K. Egilmez, L. Xiang, D. Chandra, R. G. Maunder, S. X. Ng, and L. Hanzo, "Polar Codes and Their Quantum-Domain Counterparts," *IEEE Commun. Surveys Tut.*, vol. 22, no. 1, pp. 123–155, 2019.
- [25] G. Berhault, C. Leroux, C. Jégo, and D. Dallet, "Hardware Implementation of A Soft Cancellation Decoder for Polar Codes," in *Conf. Design Architectures Signal Image Process. (DASIP)*. IEEE, 2015, pp. 1–8.
- [26] G. Tsoulos, *MIMO System Technology for Wireless Communications*. CRC press, 2006.
- [27] X. Zhu and R. D. Murch, "Performance Analysis of Maximum Likelihood Detection in a MIMO Antenna System," *IEEE Trans. Commun.*, vol. 50, no. 2, pp. 187–191, 2002.
- [28] S. ten Brink and B. Hochwald, "Detection Thresholds of Iterative MIMO Processing," in *Proc. IEEE Int. Sym. Inf. Theory*, 2002, pp. 22–23.
- [29] M. El-Hajjar and L. Hanzo, "EXIT Charts for System Design and Analysis," *IEEE Commun. Surveys Tut.*, vol. 16, no. 1, pp. 127–153, 2014.
- [30] Z. Pan, E. Li, L. Zhang, J. Lei, and C. Tang, "Design and Optimization of Joint Iterative Detection and Decoding Receiver for Uplink Polar Coded SCMA System," *IEEE Access*, vol. 6, pp. 52 014–52 026, 2018.
- [31] J. Sayir, "Measuring EXIT Charts of Low Complexity Decoders," in *Int. Symp. Commun. Theory and App.(ISCTA 2009), Ambleside, UK*, 2009.
- [32] J. Lin, C. Xiong, and Z. Yan, "Reduced Complexity Belief Propagation Decoders for Polar Codes," in *IEEE Workshop Signal Process. Syst. (SiPS)*. IEEE, 2015, pp. 1–6.
- [33] C.-Y. Hung and T.-H. Sang, "A Sphere Decoding Algorithm for MIMO Channels," in *IEEE Int. Symp. Signal Process. Inf. Technol.* IEEE, 2006, pp. 502–506.
- [34] J. F. C. León, U. P. Rico, and E. Stevens-Navarro, "Complexity-Improved Sphere Decoder for MIMO Systems Using PSK Modulations," *Procedia Technol.*, vol. 3, pp. 52–60, 2012.